Spectral seismic interferometry: Efficient monitoring of unbiased seismic velocity changes at high temporal resolution

Non-peer reviewed preprint submitted to EarthArXiv

Christoph Sens-Schönfelder
GFZ Helmholtz Centre for Geosciences, Potsdam, Germany
sens-schoenfelder@gfz.de

submitted to *Geophysical Journal International*

keywords coda wave Interferometry – seismic interferometry – ambient seismic noise – subsurface monitoring – spectral monitoring.

Summary

Ambient noise based monitoring of subsurface velocity changes does not require the explicit retrieval of Green's functions by correlation. Velocity variations can directly be observed from the fluctuations in the spectrograms of ambient noise time series or their cross-spectra. This approach is more resource efficient than the conventional Green's function based monitoring and ideally suited for edge processing and the analysis of large volumes of data for example from fibre-optic records. The spectral fluctuations result from wave propagation in the heterogeneous subsurface and interference between different scattering paths. The fluctuations are directly related to the occurrence of coda waves in the Green's function. In contrast to coda wave interferometry in the time domain, monitoring the evolution of spectral fluctuations allows for measurements of velocity changes that are unbiased by changes in the source spectrum. Recognizing that the imprint of the subsurface heterogeneity is directly encoded in the spectral fluctuations opens a new perspective on the investigation of subsurface scattering and attenuation.

1 Introduction

Seismic velocities are usually considered a stationary property of the subsurface materials. Tomographic studies are useful because the spatial differences that usually amount to a few percent are larger than temporal variations. Measuring temporal changes was facilitated by leveraging the high sensitivity of scattered coda waves resulting from their long travel time that accumulates changes (Poupinet et al. 1984). This high sensitivity of long travel times has two significant consequences arising from the quasi random nature of coda waves. Since the small scale medium structure that generates the coda waves (Sato et al. 2012) cannot be resolved deterministically, the coda waveforms cannot be compared to model predictions. Measurements are thus only possible with respect to some observed reference signal with an identical source. Poupinet et al. (1984) and Ratdomopurbo & Poupinet (1995) showed that repeating earthquakes—so-called doublets or multiplets—excite nearly identical waveforms and can be used to infer the relative change in propagation velocity that occurred in between the quakes. Snieder et al. (2002) applied the idea to a rock specimen in the laboratory where active repeatable sources can be used and coined the term *Coda Wave Interferometry* (CWI). Details of how the coda signal changes in response to changes in the sources, changes in scatterer properties or changes in the propagation velocity were studied by Snieder (2006). The second consequence of the quasi-random nature of coda waves is that the spatial sensitivity of an observation can only be calculated statistically based on assumptions about the heterogeneity of the medium (Pacheco & Snieder 2005, 2006; Larose et al. 2010; Obermann et al. 2013; Kanu & Snieder 2015; Zhang et al. 2021; Dinther et al. 2021; Zhang & Sens-Schönfelder 2022).

A fundamental limitation of CWI for field applications is the need for repeatable sources. Though active sources had been used (Yamaoka et al. 2001; Yamamura et al. 2003; Wegler et al. 2006) the real breakthrough for monitoring of temporal velocity variations was achieved by combining CWI with Greens's function retrieval from ambient seismic noise (Sens-Schönfelder & Wegler 2006). Since then, noise based CWI—or *Passive Image Interferometry* has been applied to monitor volcanoes (Brenguier et al. 2008; Sens-Schönfelder et al. 2014; Makus et al. 2024), fault zones (Wegler & Sens-Schönfelder 2007; Brenguier et al. 2014), environmental changes related to temperature (Sens-Schönfelder & Larose 2010; Gassenmeier et al. 2015; Lindner et al. 2021) and hydrology (Wang et al. 2017; Illien et al. 2021; Mao et al. 2022) as well as subsurface material damage (Illien et al. 2023) or Earth tides (Takano et al. 2014; Sens-Schönfelder & Eulenfeld 2019).

One of the difficulties with the noise based monitoring is the separation of changes in the signals that are due to changes in the subsurface and changes that are introduced in the signals due to changes in the ambient noise field. Seismic interferometry (Curtis et al. 2006) guarantees the convergence to the Green's function only under ideal conditions that are rarely met in reality. Changes in source locations or power spectrum introduce a bias in retrieved signals that can lead to misinterpretations if the bias is system-

atic and does not just add random fluctuations to the results (Zhan et al. 2013). Furthermore the Passive Image Interferometry is a resource intensive method since continuous seismic records need ot be obtained, correlated and stored in order to perform the monitoring.

In this work I address these two issues by performing the ambient noise based subsurface monitoring in the spectral domain. I show in section 2 how CWI can be transferred to the spectral domain. In section 3 I demonstrate that a potential bias resulting from changes in the source power spectrum can be avoided or reduced in the spectral domain. Computational demands of Passive Image Interferometry are addressed in section 4 where I show that if the monitoring is performed on the amplitude spectrum one can do so directly on the ambient noise trace without the need explicitly retrieve the time domain Green's functions. Conditions and consequences of the spectral monitoring are discussed in section 6 before I conclude with section 7.

2 Measuring velocity changes with coda waves

Absolute seismic wave velocity in the subsurface is estimated from travel time measurements for a known path. Velocity *changes* can be estimated from variations of travel times even without knowledge of the actual length of the path travelled by the wave provided that source and receiver locations are identical. If the relative velocity change is spatially homogeneous the true velocity change can be measured, otherwise an apparent change is obtained that represents a residence time average along the path.

In the case of a spatially homogeneous relative velocity change the effect on the Green's function is given by the transformation

$$\mathcal{T}(\xi) : g(\tau) \rightarrow g(\xi\tau) = g'(\tau) \ . \tag{1}$$

Here g and g' are the original and the perturbed Green's functions, τ is lapse time and ξ is the stretching factor that is related to the perturbed velocity v' and original velocity v by

$$v' = \frac{1}{\xi} v \ . \tag{2}$$

The commonly used relative velocity change dv/v is related to ε by

$$\frac{dv}{v} = \frac{v' - v}{v} \approx \varepsilon := -\log(\xi) \ . \tag{3}$$

This definition of ε has the advantage of being reversible, i.e. $\mathcal{T}(\xi(-\varepsilon))\mathcal{T}(\xi(\varepsilon)) : g = g$ (cf. Makus & Sens-Schönfelder 2024).

For CWI scattered waves with a range of lapse times τ are used to obtain accurate estimates of ε. To quantitatively estimate velocity changes with CWI, essentially any coda based monitoring study uses one of two (or both) methods that we call *moving time window* or *stretching* technique in accordance with Sens-Schönfelder & Brenguier (2019).

2.1 Moving time window and stretching methods

Before discussing the methods of velocity estimation let us introduce a model for recorded seismograms, which combines effects of the medium and the source. It will help to illustrate how to separate medium and path effects later. We model the Green's function $g(\tau)$ as a sequence of randomly located delta functions with decaying amplitudes that represent the arrivals of scattered waves similar to a reflectivity function (Fig. 1a). The source wavelet $s(\tau)$ is a much shorter signal that is convolved with the Green's function to obtain the recorded seismogram $u(\tau)$ (Fig. 1b, c):

$$u(\tau) = g(\tau) * s(\tau) \ . \tag{4}$$

The aim of coda wave based monitoring is to measure a velocity change described in 1 that acts on the Green's function from the recorded signal u given in 4.

The moving time window technique uses multiple short time windows centered at different lapse times τ_i and estimates the time shift $\Delta\tau_i$ that maximizes the fit between the $g(\tau_i)$ and $g'(\tau_i + \Delta\tau_i)$ in these time windows. According to 1

$$\frac{\Delta\tau_i}{\tau_i} = \xi_i - 1 \tag{5}$$

and one can obtain an estimate ξ as an average over multiple time windows:

$$\xi = \bar{\xi_i} \ . \tag{6}$$

This approach has been introduced by Poupinet et al. (1984) who estimated $\Delta\tau_i$ from phase shifts in the spectral domain while Snieder et al. (2002) maximised the shifted correlation in time domain. The duration T of the time windows has to be short, such that $(\xi - 1)T \ll 1/f_{max}$ to ensure that the distortion of the waveform within the time windows remains small compared to the shortest period $(1/f_{max)})$ of the signal.

The stretching method was introduced by Lobkis & Weaver (2003) and Sens-Schönfelder & Wegler (2006) and avoids the necessity of short time windows by directly simulating the stretching in time domain. It maximizes the fit between $u(\tau)$ and $u'(\xi\tau) = g'(\tau) * s(\tau)$ where the latter is created by interpolating u' at the new sampling points τ/ξ. Since the duration of the time window can be much longer, the stretching method reduces the risk of cycle skipping and usually provides more stable estimates of the velocity change than the moving window method (Hadziioannou et al. 2009). The fit of the waveforms $u(\tau)$ and $u'(\xi\tau)$ is usually quantified by means of the correlation:

$$C(\xi) = \frac{\int_T u(\tau)u'(\xi\tau)d\tau}{\sqrt{\int_T u(\tau)^2 d\tau \int_T u'(\xi\tau)^2 d\tau}} \ . \tag{7}$$

Since the stretching is performed on u instead of g to estimate ξ, the source time function s is implicitly stretched, too. Zhan et al. (2013) raised the concern that this implicit stretching of the source signal would lead to a bias in estimates of velocity changes with the stretching method by mapping real source changes into stretching that could then be wrongly interpreted as resulting from velocity changes.

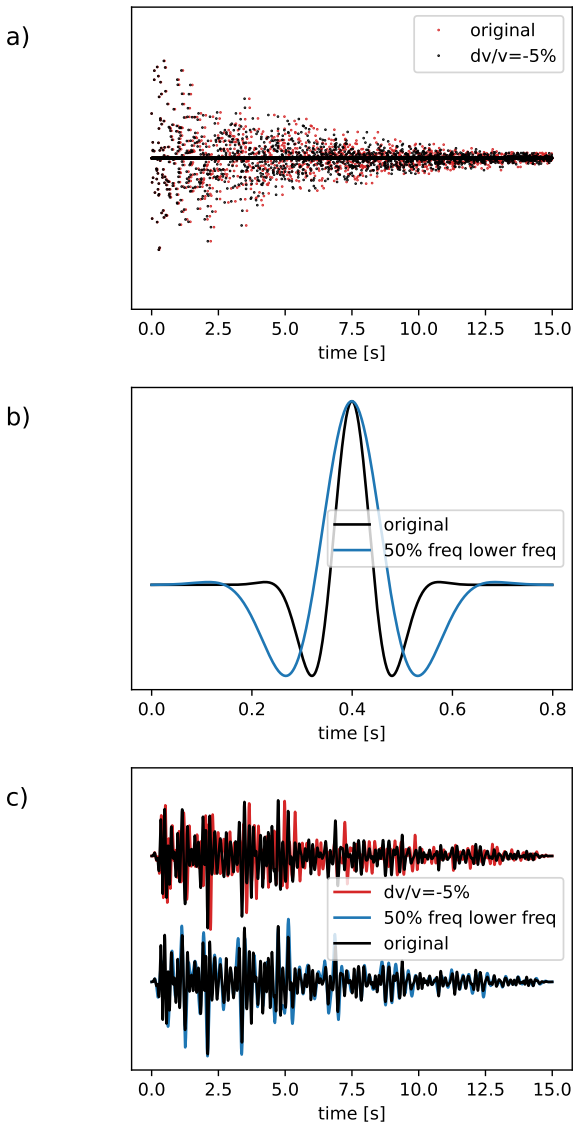

Figure 1 Model for a recorded seismic coda signal. a) Sequence of delta functions representing the medium's Green's function. Only the maxima of the delta spikes are shown for clarity. The situation of a stretched sequence for a state with 5% lower velocity is shown in red. b) Source time function that excites the medium. Blue shows a source time function with 50% reduced frequency. c) Resulting signals of the Green's function convolved with the source time function for a change in velocity (top) and a change in source frequency (bottom) as illustrated in a) and b) respectively.

A possibility to circumvent the unintended mapping of source changes into estimated velocity changes is to work in the spectral domain.

2.2 Equivalence of stretching in time and frequency domain

Let $g(\tau)$ be the Green's function from some source location to some receiver as defined above. Its Fourier transform is

$$\hat{g}(\omega) = \int g(\tau) e^{i\omega\tau} d\tau \ . \tag{8}$$

Let us again assume a spatially homogeneous change of the wave velocity resulting in a stretching of the Green's function $g'(\tau) = g(\xi\tau)$. The spectrum of the stretched Green's function is

$$\begin{aligned} \hat{g}'(\omega) &= \int g'(\tau) e^{i\omega\tau} d\tau \\ &= \int g(\tau') e^{i\omega\frac{\tau'}{\xi}} \frac{1}{\xi} d\tau' \\ &= \frac{1}{\xi}\hat{g}\left(\frac{\omega}{\xi}\right) \end{aligned} \tag{9}$$

where we used the substitution $\tau' = \tau\xi$. This shows that stretching in time domain is equivalent to a compression (inverse stretching) of the complex spectrum with an additional scaling by $1/\xi$. Stretching in time domain by ξ corresponds to a stretching in frequency domain by $1/\xi$. In some implementations of the stretching method this correspondence is implicitly used to create stretched versions of the reference trace by appending zeros to the spectrum which results in a resampling of the frequency axis. Up to my knowledge the only study that explicitly estimated velocity changes by stretching of the spectrum in frequency domain is Dai et al. (2013). The correspondence between velocity changes and stretching in time (eq. 3) and frequency domain can thus be extended to

$$\frac{dv}{v} = -\frac{d\tau}{\tau} = \frac{df}{f} \ . \tag{10}$$

Fig. 2 illustrates the stretching of the spectrum. It shows the real and imaginary parts of the traces in Fig 1c. As described by (9) the stretching of the time series due to a reduced velocity compresses the spectrum moving the spectral patterns to lower frequencies. Since the phase of the spectrum is rapidly varying, the velocity change can be independently estimated from the real or the imaginary part of the spectrum.

3 Separating source and path effects in the spectral domain

3.1 Phase Spectrum

Alternatively to the complex spectrum the stretching can be evaluated in terms of the amplitude $a(\omega)$ and phase spectrum $\phi(\omega)$:

$$\hat{g}(\omega) = a(\omega) e^{i\phi(\omega)} \ . \tag{11}$$

The phase spectrum is strongly fluctuating and subject to jumps of 2π from phase wrapping as shown in Fig. 3a. Stretching thus not be done by simple interpolation of the phase spectrum but requires an upsampling in the frequency domain. The upsampling can easily be achieved by zero-padding the timeseries prior to the Fourier transform. An example of an enlarged section of the phase spectrum is shown in Fig. 3b for the original trace u, the trace obtained with perturbed velocity and a stretched version of the original phase spectrum.

The phase spectrum has an interesting advantage in comparison to the time domain and the amplitude spectrum. As Zhan et al. (2013) showed there is a possibility that changes

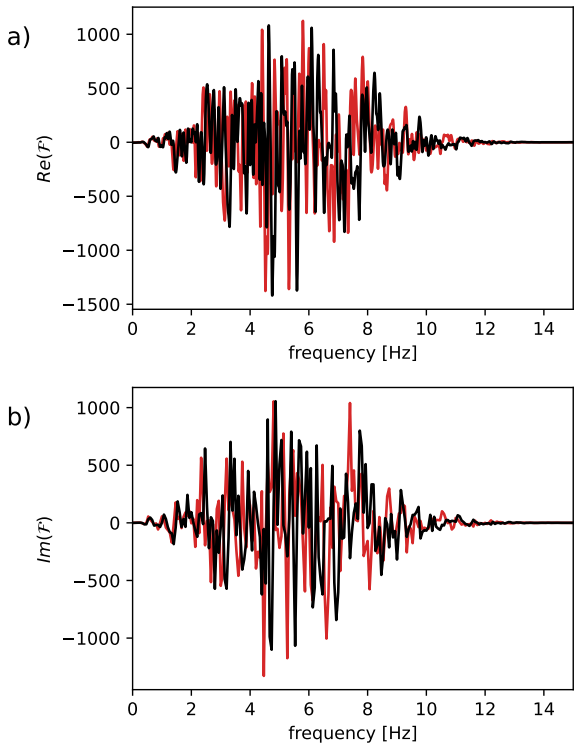

Figure 2 Stretching of the complex spectrum (real part: a, imaginary part: b) resulting from the velocity change underlying the signals shown in Fig. 1c. The stretching of the time series leads to a compression of the spctrum.

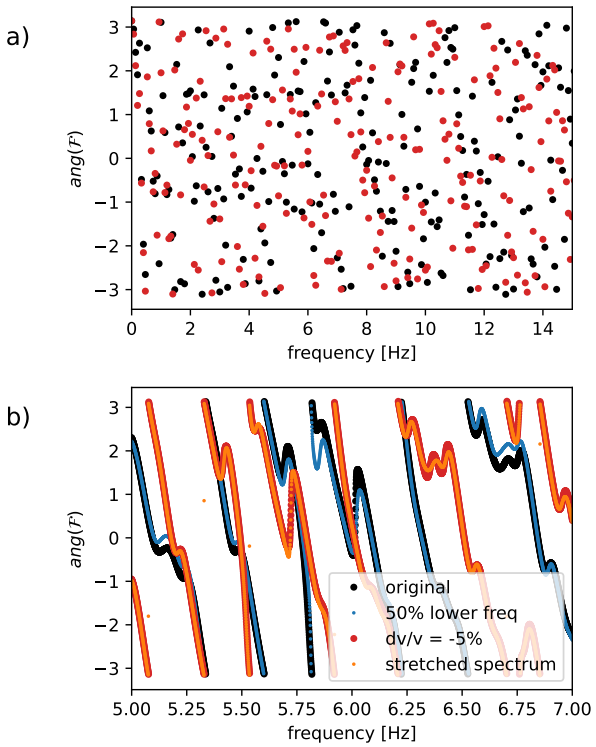

Figure 3 Effect of velocity and source frequency changes on the phase spectrum. a) Phase spectrum of the original signal and the signal resulting from a 5% velocity reduction at common spectral resolution. b) Interpolated phase spectra in a narrow band. Shown are the original signal and the signal with 50% lower source frequency in black and blue, respectively. The curves are mostly identical since the source frequency change of the zero-phase source does not affect the phase of the signal. The phase of the signal with the 5% reduced velocity is shown in red. It is overlain by the orange curve that shows the original signal compressed by 5% to simulate the effect of the velocity change.

in the amplitude spectrum of the source map into time domain stretching. But how does this affect the phase spectrum? For impulsive sources a change in the amplitude spectrum is linked to changes in phase. However, because of the temporal coverage most coda wave monitoring studies are based on Green's function estimates retrieved via Seismic Interferometry (Curtis et al. 2006) from ambient noise correlation functions (Sens-Schönfelder & Brenguier 2019). In frequency domain the correlation of noise traces results in a signal that represents the difference of the advanced and retarded Green's functions multiplied with the power spectrum of the noise source time function (Snieder & Larose 2013). Since the phase of the power spectrum is zero, the effect of changes in the spectrum of the noise source will be limited to the amplitude spectrum of the retrieved correlation function, while the phase spectrum is unaffected (cf. Fig 3b). The phase of the correlation function is thus dictated solely by the Green's function of the medium. Stretching of the phase spectrum thus provides an unbiased estimate of velocity changes in the propagation medium.

This property of the phase spectrum has been used as an argument in favor of the moving time window method. So, how is it related to phase stretching? The original formulation of the moving time window method by Poupinet et al. (1984) estimated the time shift of waveforms in the short time windows from their phase difference $\Delta\phi = \omega\Delta\tau$ where $\Delta\tau = (\xi - 1)\tau$ it the arrival time difference at arrival time τ. On the other hand the phase difference caused by the stretching is $\Delta\phi = (\xi - 1)\omega\frac{\partial\phi}{\partial\omega}$. Both expressions are equal for $\tau = \frac{\partial\phi}{\partial\omega}$, i.e. non-dispersive waves which corresponds to the requirement of short time windows.

3.2 Amplitude spectrum

As shown above also the amplitude spectrum of recorded signals can be used to estimate changes in the propagation medium. Naturally the amplitude spectrum of a recorded signal reflects changes in the spectrum of the source signal. This also holds for noise correlation functions where spectral changes are expected for example between the seasons (Ardhuin et al. 2011; Hillers & Ben-Zion 2011). In Fig. 4a we show the amplitude spectrum of the three signals from Fig. 1c where it is easy to recognize the stretching between the two graphs representing the spectra original signal and the 5% stretched signal. Unfortunately the amplitude spectra mix the influence of source and propagation. The spectrum of the signal affected by the 50% decrease in source frequency has a significantly different shape in Fig. 4a.

However, while Green's function and source time function are convolved in the time series they are multiplied in frequency domain where their effects can be more easily

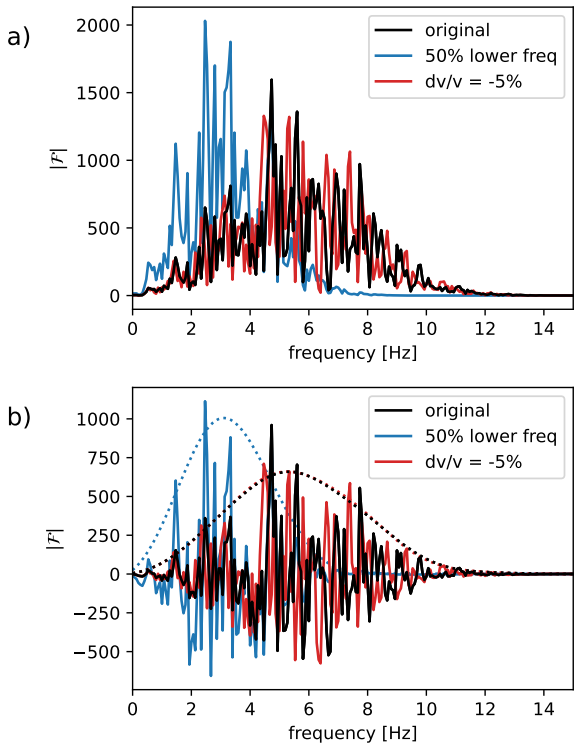

Figure 4 Effect of velocity and source frequency changes on the amplitude spectrum. a) amplitude spectra, b) separation of amplitude spectra. The smooth part of the spectra is indicated with dashed lines and the fluctuating part with continuous lines. Colours indicate the original signal (black), a signal with 50% lower source frequency (blue) and a signal resulting from 5% velocity reduction (red).

separated. As illustrated in the model used in Fig. 1 the Green's function usually is a long time series with randomly occurring arrivals resulting in a broad spectrum with rapid fluctuation. The source time function on the other hand is a much shorter time series leading to a smooth spectrum that is usually limited in bandwidth. In consequence the spectrum of the recorded signal is a rapidly fluctuating spectrum that is modulated by a smooth band-limited envelope. By extracting the rapidly fluctuating part of the amplitude spectrum one can thus extract the effect of the path and separate it from the source effect.

Figure 4b shows how the source and path effects can be separated. A simple high-pass filter is applied to the amplitude spectra in Figure 4a in order to extract the rapidly oscillating part that fluctuates with more than 0.25 oscillations per Hz or equivalently those, whose fluctuation in frequency domain are shorter that 4 Hz. This filter limit is an inverse frequency that corresponds to the bandwidth of the source signal, which is roughly 4 Hz in the present example. Figure 4b shows the rapidly fluctuating and smoothly varying parts of the original trace, the trace resulting from a 5% velocity change, and a 50% decrease of the source frequency. It is clear that the velocity change affects the location of peaks and troughs while the peaks and troughs of the signal affected by the source change overlay exactly with those of the original signal.

Since the amplitude of the fluctuations in the spectra are

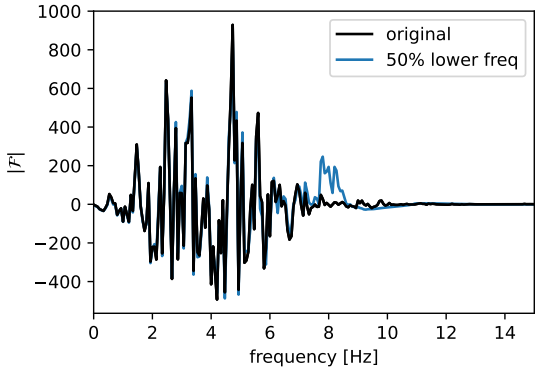

Figure 5 Amplitude spectra corrected for changes in the source spectra represented by the smooth part of the spectra (dashed lines in Fig. 4).

roughly proportional to the source energy, the peak to peak amplitude changes with the source spectrum. Fig.5 shows that this can easily be corrected by a normalization. The rapidly varying parts of the spectra are normalized by the respective smooth parts and scaled with the geometric mean of the smooth parts of the two different source signals. Scaling with the geometric mean is useful to taper off spectral bands in which one of the signals has vanishing energy. The agreement of the two curves in Fig.5 shows that despite significantly different source spectra one can retrieve the spectral signature of the propagation medium from the amplitude spectrum of a seismic signal.

4 Estimating velocity changes from noise amplitude spectra

In section 3 above I show how a velocity change in the propagation medium can be retrieved from changes in the spectrum of a recorded seismic signal of an isolated source. This is analogous to coda wave interferometry in frequency domain. For a zero phase source signal as it is the case in noise correlation functions, the phase spectrum can be used to obtain a signal that is unbiased from changes in power spectrum of the source. Also from the amplitude spectrum a signal that is unbiased by source changes can be retrieved by extracting the fluctuating part.

However, another advantage of the spectral approach becomes apparent in the context of ambient noise based monitoring with seismic interferometry. In Passive Image Interferometry the signal that is used for monitoring is not directly recorded, but retrieved from ambient noise by cross-correlation of the ambient field vibrations. The frequency domain Green's functions for acoustic waves can be written as:

$$\hat{g}(r_A, r_B; \omega) + \hat{g}^*(r_B, r_A; \omega) = 2i\omega \int_{\partial V} \frac{1}{\rho(x)v(x)} \hat{g}(r_A, r; \omega)\hat{g}^*(r_B, r; \omega) dS \quad (12)$$

(Snieder et al. 2007). Here $\hat{g}(r_A, r_B; \omega)$ is the Green's function for propagation from location r_B to r_A. Sources at locations r are on the boundary ∂V of the volume containing

A and B. ρ and v are density and acoustic velocity, respectively and * denotes complex conjugation. We know from equation 9 that a velocity change in the medium results in a stretched Green's function, i.e. $\hat{g}'(\cdot,\cdot,\omega) = \hat{g}(\cdot,\cdot,\omega')/\xi$ for $\omega' = \omega/\xi$. It is clear from equation 12 that a stretched Green's function $\hat{g}(r_A, r_B, \omega')$ on the left hand side can be easily obtained if also the Green's functions on the right hand side are stretched, i.e. $\hat{g}'(r_A, r, \omega)$ and $\hat{g}'(r_B, r, \omega)$. In the case of a homogeneous velocity change in V the propagation from ∂V to the receivers r_A and r_B is affected by the same velocity change such that: $\hat{g}'(r_{A,B}, r, \omega) = \hat{g}(r_{A,B}, r, \omega')/\xi$. In this case we have

$$\hat{g}'(r_A, r_B; \omega) + \hat{g}'^*(r_B, r_A; \omega) = 2i\omega' \frac{1}{\xi^2} \int_{\partial V} \frac{1}{\rho(x)v(x)} \hat{g}(r_A, r; \omega')\hat{g}^*(r_B, r; \omega')dS \ . \quad (13)$$

If the sources are far away from both stations and the velocity change in the propagation medium is spatially heterogeneous in between the location of the sources and region of interest, the frequency stretching with the correct stretching factor does not occur for each Green's function in the integrand separately, but only for their product, i.e. their cross-spectrum which is equivalent to the time domain correlation. This ensures that the signal of the travel time *differences* is stretched and not the original travel times.

This discussion shows that instead of using seismic interferometry to measure seismic velocity change from ambient noise cross correlations, one can observe a velocity change directly from their cross spectrum. This means that a velocity change can directly be measured from the cross-spectrum of the noise without the need for an inverse Fourier transform to retrieve the time domain Green's function, hence reducing the computational costs. For autocorrelations with $r_A = r_B$ one can estimate a velocity change in the propagation medium directly form the spectrogram of the noise.

5 Examples of velocity changes

To demonstrate that the proposed method to measure velocity changes directly from the noise amplitude spectra works in practical applications I show selected examples from three different environments. Two of these examples are re-processed datasets for which velocity changes measured with conventional passive image interferometry are available in the literature.

5.1 Inter eruptive changes at Kilauea

As a first application I discuss data from Kilauea volcano (Hawaii) where source and medium changes are superimposed. Kilauea entered an active period in December 2024 and generated a series of hour long eruptions with vigorous fountaining. The eruptive phase produced a spectral signature that reflects the gliding dominant tremor frequency and subsurface velocity changes at the same time. Fig. 6 shows data from station WRM of the HV Hawaiian-Observatory network (USGS Hawaiian Volcano Observatory (HVO) 1956) for 15 days of an inter-eruptive episode

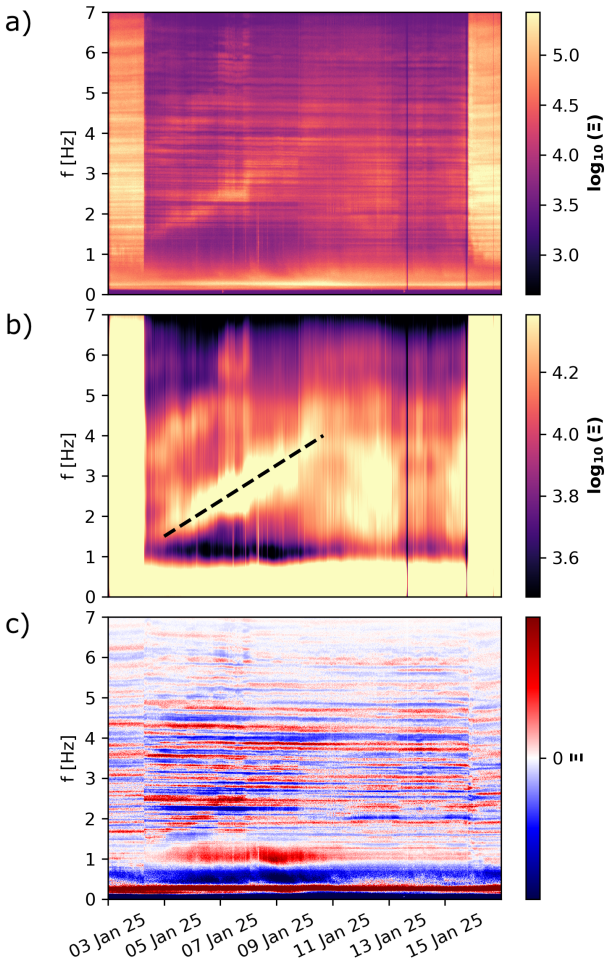

Figure 6 Decomposition of the cross-spectrogram between the vertical and north component form an inter-eruptive episode at Kilauea. a) raw spectrogram. b) smooth part of the spectrogram with less than one fluctuation per Hertz. The dashed line indicates the gliding of the dominant source frequency c) normalized fluctuating part of the spectrum with more than one fluctuation per Hertz. Colour scales in a and b are logarithmic.

in January 2025. The spectrogram of the seismic signal are shown in Fig. 6a. More precisely it is the amplitude of cross spectrum (Ξ) between the north (u_N) and vertical (u_Z) components:

$$\Xi(\omega) = |\hat{u}_N(\omega)\hat{u}_Z^*(\omega)|^{\frac{1}{2}} \ . \quad (14)$$

The Fourier transform is applied to 2048 samples long windows at 20Hz sampling frequency, i.e. approximately 100s long segments with 50% overlap. I show the cross spectrum only for demonstration. Other cross spectra and individual component amplitude spectra have the same properties.

Fig. 6b shows the smooth part of the spectrogram and clearly indicates the high energy at low frequency due to ocean microseisms and the high energy levels at all frequencies during the eruptions in early and mid January. The tremor with the gliding frequency that increases from 1.5Hz to about 4Hz over the course of five days is indicated by the dashed line.

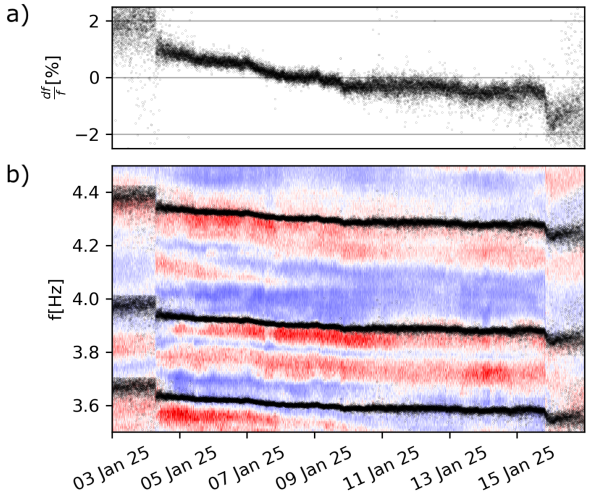

Figure 7 Relative frequency changes of the fluctuating part of the spectrogram at 100s resolution. a) relative frequency change estimated with the stretching method in the 1.5Hz-5Hz band. b) Close-up of the spectrogram with superimposed estimates of frequency changes.

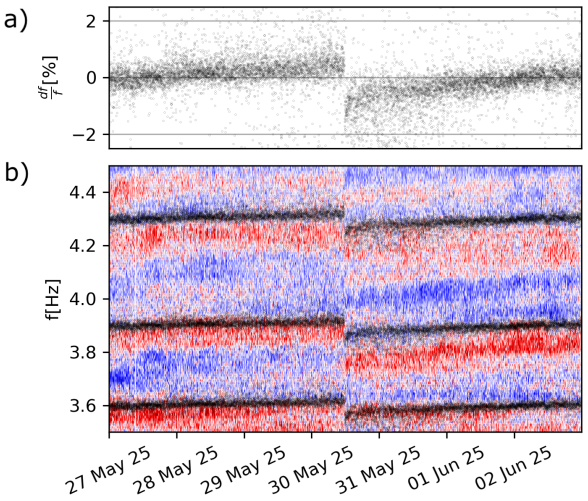

Figure 8 Same as figure 7 for the time around a local earthquake at noon on May 30 2025.

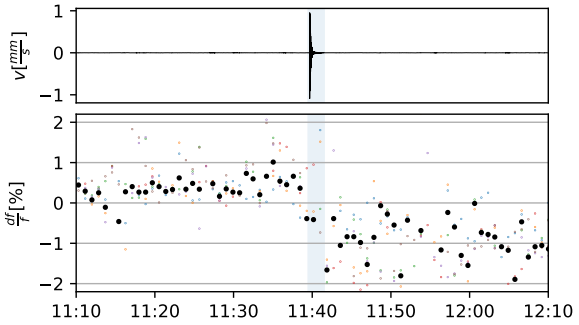

Figure 9 Close-up of the time around the local earthquake on May 30,2025. a) Vertical velocity seismogram. b) frequency changes showing the instant and persistent drop of the relative frequency.

The fluctuating part of the spectrogram is shown in Fig. 6c. The striations of persistent peaks and troughs are clearly visible across times of drastically changing source spectra due to the normalization described in section 3.2. Note that the colour scale of Fig. 6a and b is logarithmic, while it is linear in c. A close look at the pattern in Fig. 6c reveals variability in the fluctuations as it is expected for velocity changes in the propagation medium, i.e. a stretching of the spectrum. This variability is quantified with the stretching technique Sens-Schönfelder & Wegler (2006); Hadziioannou et al. (2009) and illustrated in in Fig. 7a. It show that the fluctuating part of the cross-spectrum is compressed by more than 1% between January 4 and 10. Fig. 7b illustrates this compression of the spectrum with a close-up around 4Hz and superimposed evolution of the spectral lines as predicted form the measured df/f in a. According to section 2.2 the frequency stretching is the inverse of the corresponding stretching of the time series which means that the observed relative frequency changes is equal to an underlying relative velocity changes: $\frac{df}{f} = \frac{dv}{v}$.

Interestingly the compression (i.e. the transition to lower frequencies) of the fluctuating spectrum occurs at the same time when the smooth part of the spectrum shows an increase in frequency of the peak. The source and path path effects can be clearly separated.

5.2 Co-seismic changes at Kilauea

The velocity changes inferred above occur during a phase when the ambient wavefield changes quite strongly due to the volcanic origin of the sources. To add further confidence that the fluctuating part of the spectrum reflects the subsurface wave propagation rather than the source properties, we investigate velocity changes that are not related to dynamics of the volcanic sources. The most suitable signals to analyse are co-seismic changes.

The first example in Fig. 8 shows a shallow (0.9km) Ml=2.8 event that occurred on 2025-05-30 11:39:38 (UTC) at a distance of about 3km from station WRM. A clear compression of the fluctuating spectrum is visible on May 30 that corresponds to a velocity drop of 1%. Again the changes can be readily observed in the spectrogram.

A close-up in Fig. 9 shows one hour around the drop at a 1-minute time resolutions together with the vertical component seismogram. Coloured dots indicate measurement from the six different spectra and cross-spectra, while the black dots show the joint estimate form all components. There is 50% overlap of the time windows. At the time of the earthquake a fairly stable estimate of the frequency change is interrupted and estimates stabilise after the event at 1% relative decrease and with slightly larger scatter. The two time windows containing the event have much larger error.

As a second example we show the response to teleseismic body wave excitation from the 609km deep Mw 8.3

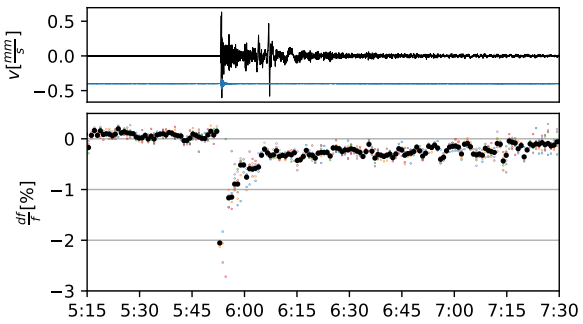

Figure 10 Relative frequency change in response to the excitation by the Sea of Okhotsk earthquake in 2013. a) broad band ground motion velocity in black and in the 1.5-5Hz band used for estimation of the frequency changes in blue with offset. b) relative frequency changes as in Fig 9.

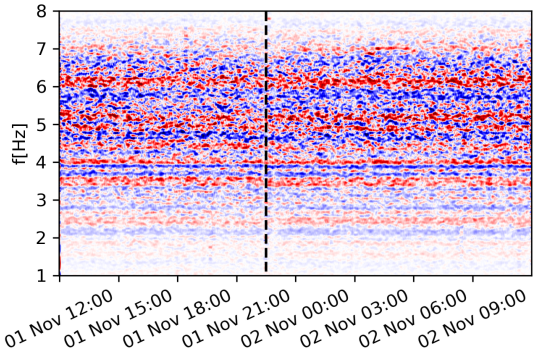

Figure 11 Fluctuating part of the vertical component spectrogram of station 7F.PA46. Segments containing earthquake signals have been removed with the method described in Illien et al. (2023). The dashed line indicates the time of the earthquake.

Sea of Okhotsk earthquake that occurred on May 24, 2013. In contrast to the local event there is no possibility for this event to induce static stress changes or any other temporally correlated process that could affect the local seismic velocities. As shown in Fig. 10 the strong first arriving P-wave caused a sharp drop that began to recover immediately but persisted for several hours. The excitation by the teleseismic waves in the frequency band used for the measurements lasted only for a few minutes (blue line in Fig. 10a) while the lower frequency oscillations lasted much longer (Sens-Schönfelder et al. 2015). To my knowledge this is the first observation of seismic velocity changes caused by teleseismic waves. In this particular case of a very deep source the changes are caused by P-waves.

5.3 Observations in non-volcanic environments

Since changes in the amplitude spectrum have mostly been observed at volcanoes (Yates et al. 2026) I show another example here, that demonstrates the method in a non-volcanic setting of northern Chile at the IPOC station CX.PATCX (GFZ German Research Centre For Geosciences & Institut Des Sciences De L'Univers-Centre National De La Recherche CNRS-INSU 2006). We observed temporal changes at this station before (Richter et al. 2014; Gassenmeier et al. 2016; Sens-Schönfelder & Eulenfeld 2019) which responds in a rather predictable way to seismic excitations (Illien et al. 2025). Illien et al. (2023) investigated a period when the permanent station was surrounded by an array of nine stations in the 7F network (Sens-Schönfelder 2023) to improve the monitoring. A $M_w 6.2$ event at 150 km distance was recorded by the array and caused a 0.4% velocity drop (Illien et al. 2023). Figure 11 shows the fluctuating part of the vertical component spectrogram of station 7F.PA46 at a 10 minute resolution. Events have been removed as described in Illien et al. (2023) by setting the segments affected by earthquakes to zero. As before persistent peaks can be observed that allow to monitor the coseismic 0.4% velocity drop identified by Illien et al. (2023). However, the co-seismic changes are too small to be directly observed in the spectrogram. In Figure 12 a heat map of the changes observed on the 465 component combinations provided by the local network and their median is shown, again with a 10 minute resolution. It clearly shows the co-seismic velocity reduction. The period around 15:00 - 18:00 UTC, i.e. early afternoon, locally, is regularly influenced by elevated wind activity that causes additional noise, a loss of correlation and larger scatter of df/f on some of the temporary installed stations (Illien et al. 2023).

As a last example I show data from Nepal that was analysed by Illien et al. (2021) and Illien et al. (2022). The noise is recorded by stations of the *Landscape Response to the Mw7.9 Gorkha Earthquake*- network (Andermann et al. 2015) on a terrace next to the Bhote Koshi river. Here the ambient vibrations above 1Hz are dominated by the river and has very different origin than in the previous examples with noise originating from volcanic and marine sources. Using ambient noise correlation Illien et al. (2021) observed large seasonal velocity variations amounting to several percent between dry and wet seasons. A hydrological model provided very detailed explanation of the velocity variations solely based on independently measured precipitation confirming the origin of the changes in the propagation medium. Figure 13 shows the fluctuating part of the spectrogram and the measured relative frequency changes. They perfectly track the velocity changes observed by Illien et al. (2021) and Illien et al. (2022) despite significant changes in the river noise during the monsoon seasons.

6 Discussion

Using a synthetic example in section 3 I show how the estimation of medium changes in the frequency domain can help to improve monitoring of wave velocity changes. While the source and path effects are convolved in time domain and difficult to separate, they are multiplied in frequency domain and can be separated under certain assumptions. Two strategies are presented that rely on different properties of the phase and amplitude spectrum. In signals retrieved with seismic interferometry the correlation of the ambient vibration signal causes the phase spectrum of the

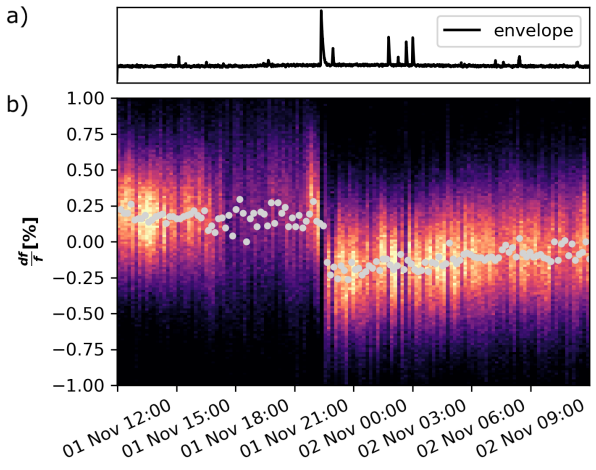

Figure 12 Relative frequency changes observed by the local array around station PATCX in in northern Chile. a) envelope of the vertical component velocity at PATCX in the frequency band from 1 to 8 Hz. b) heat map of relative frequency changes observed from the 465 possible component combinations in the array and their median shown be grey dots.

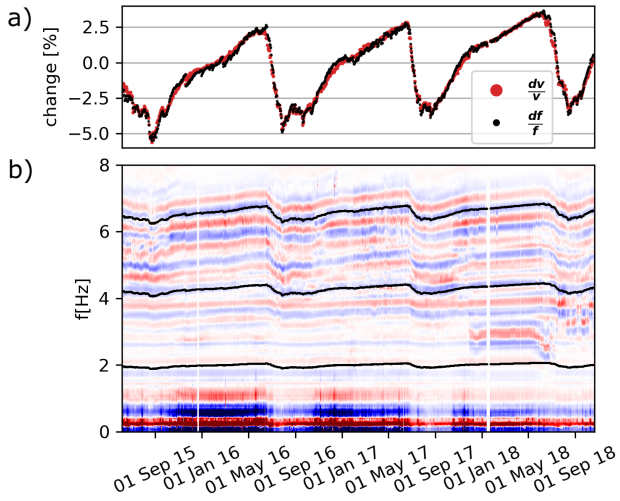

Figure 13 Relative frequency changes at the Chaku site in Nepal. a) Relative frequency changes of all cross- and amplitude spectra averaged from station NEP10 in black. Red dots (mostly covered) show the relative velocity changes of Illien et al. (2022). b) fluctuating part of the spectrogram of the vertical channel of station NEP10 with superimposed absolute frequency changes at selected frequencies.

source to vanish–only the power spectrum of the source signal affects the retrieved Green's functions. This means that the phase spectrum of a noise correlation function is unaffected by source changes and reflects the properties of the propagation medium. It thus allows for an unbiased estimate of velocity changes.

In contrast the amplitude spectrum of a signal is affected by the source spectrum even when retrieved from ambient field correlations. However, one can assume that the autocorrelation function of the source signal is shorter than the duration of the Green's function–an assumption that is implicit in most applications that use coda waves. Otherwise the coda would represent the source signal rather than the medium response. This combination of a short source signal and a long and random (non-repeating) medium response allows to separate both contributions by filtering the spectrum into a smooth and a fluctuating part for both contributions, respectively. Of course the fluctuating part does not perfectly represent the amplitude spectrum of the Green's function, as demonstrated in section 3.2, since it fluctuates around zero and can be negative. However, this is irrelevant here, since we aim to extract temporal changes and not the Green's function itself. Accurate estimates of temporal changes that are unbiased by source frequency changes can thus be obtained from the fluctuating part of the amplitude spectrum.

The real advantage of the spectral estimation of medium changes, however, becomes apparent when we consider that Passive Image Interferometry or noise based monitoring as we developed it 20 years ago requires a transformation of the continuous noise signal in the Fourier domain for correlation, already. This is followed by an inverse transform to obtain the Green's function in time domain from which we can estimate temporal changes either by CWI in time domain or after another Fourier transform in frequency domain, as shown above. The innovation that I propose here is that the possibility to estimate changes of the wave propagation velocity from the amplitude spectrum allows to measure these changes directly from the continuous ambient vibrations without the need for an inverse transform into time domain as required by seismic interferometry. There have been speculations about this possibility based on the similarity of temporal changes obtained from the noise spectrum at volcanoes and the retrieved Green's functions (Yates et al. 2026). Some uncertainty remained in Yates et al. (2026) about the effect of changes in the source spectra and the origin of the fluctuations in the spectrum. The correspondence between changes of individual peaks in the amplitude spectrum and material properties was also used by Compaire et al. (2022). The authors found that certain peaks in the power spectrum of the ambient vibrations recorded by the SEIS instrument of the InSight on Mars co-evolved with velocity changes inferred from repeating Mars quakes. Other peaks did show very different dynamics that was attributed to lander modes.

Realizing the possibility to estimate medium changes directly form the noise amplitude spectrum or the cross-spectra has a number of implications that deserve discussion

1. numerical requirements for monitoring medium changes from the amplitude spectrum

2. averaging properties of the amplitude spectrum are different from the averaging properties of the noise correlation functions affecting the temporal resolution

3. the spatial sensitivity of the spectrum-based measurements might differ from the noise correlations based monitoring.

6.1 Numerical advantages of spectrum-based monitoring

Noise correlation based monitoring typically works in the following sequence

1. calculation the pairwise correlation function of short time windows of ambient noise most often by Fourier transform, multiplications and inverse Fourier transform.

2. stacking of the short time correlations to obtain a stable signal and storage of the resulting stacked correlation function

3. estimation of a reference signal and measurement of the apparent velocity change with the method of choice (stretching, moving windows, wavelet)

Since the spectral method does not require the inverse Fourier transform, velocity changes can essentially be estimated on the fly without the need to store the intermediate set of correlation functions. Of course there are details to be considered especially when cross-spectra of many station combinations are to be used. It might be useful to store the spectra of individual channels to avoid recalculating them for each channel pair. To estimate changes one would then load the spectra, calculate the cross-spectrogram by multiplication of the individual spectra and estimate the velocity change. This approach reduces the storage requirements, since the spectrograms have essentially the same size as the original data, while the pairwise correlation functions can easily inflate the dataset. This is a significant advantage especially for applications in edge computing where calculations are performed directly on the sensor with limited resources. Another area where resources quickly become critical is the application to fibre optic data. Here, the computational advantage might be essential.

6.2 Averaging properties and temporal resolution

Besides the numerical advantage of the spectrum-based monitoring its performance needs to be compared to the traditional correlation-based monitoring. Yates et al. (2026) show a number of examples from volcanic environments that demonstrate the similarity between seismic velocity changes observed with traditional noise correlations and relative frequency changes observed in the spectrum. Part of the differences observed by Yates et al. (2026) might result from the fact that these authors measured shifting of the fluctuating part of the spectrum, not stretching. However, subjectively the striations of the spectrogram appear more stable over time than the pattern of the Green's functions in time domain. Exact analysis of this difference is required, but an indication is provided by comparing Figures 1c and 5. Filtering the spectra for the fluctuating part and not using the full spectrum reduces the source effect which is not possible for time domain Green's functions. This enhances the stability of the spectral estimates and is similar to the difference between interferometry by correlation and deconvolution. Nakata & Snieder (2012) compare the stability of correlation and deconvolution of borehole and surface sensors signals from earthquakes and conclude that the lack of stability in the correlation approach is due to the different power spectra of the earthquakes used in their analysis, which is accounted for only by deconvolution. I suggest that estimating changes only from the fluctuating part of the spectra has a similar effect to reduce the source imprint and improve the stability of velocity change estimates resulting in higher temporal resolution.

6.3 Spatial sensitivity

A Green's function in time domain represents travelling waves. Despite the stochastic character of coda waves normally used for monitoring, there is probabilistic knowledge of their spatial sensitivity (Pacheco & Snieder 2005; Dinther et al. 2021; Zhang et al. 2021). But what is the sensitivity of a spectral estimate? I think a good analogy to this question can be build from audible sound and acoustics in a room. A direct wave from an impulsive source is sensitive to its path, only. In frequency domain, the travel time is represented by the phase spectrum and the amplitude spectrum mostly reflects the source characteristics. Once coda waves (i.e. reflections from walls) are included the sound changes strongly and one can hear the acoustic properties of the room. In time domain the late arriving coda waves have been bouncing around, sensing the room with certain probabilities. These coda waves (i.e. repeated versions of the source) create the fluctuations of the spectrum and form the *sound* of the room. The spatial sensitivity for temporal changes of the spectral estimate is thus similar to time-domain estimate from coda waves. Hereby late coda waves correspond to rapid fluctuations in the spectrum, while less rapid fluctuations correspond to early coda.

Interestingly one can hear changes in the acoustic properties of the room not only from an impulsive source signal but also from a continuous random excitation due to the spectral analysis of our auditory system whereas the time domain estimate would require sensing, storage and interferometry. Not surprisingly the spectrum based estimate of temporal changes means analysing the sound/tone of a structure.

6.4 Conditions for applicability

To understand under which conditions it is possible and advantageous to perform the monitoring of temporal changes on the fluctuations of the amplitude spectrum of the noise rather than on noise correlation functions it is important to understand the origin of the spectral fluctuations.

Spectral lines have be observed predominantly in volcanic environments where the occurrence of such stable spectral features have often been attributed to volcanic tremor, i.e. a resonance of the source process or a structure close to the source (Chouet 1996). To investigate this connection Bracale et al. (2025) constructed a complicated structural model resembling a subsurface volcanic structure and performed wave field simulations in this heterogeneous model. While the ballistic waves in their simulations have a rather smooth spectrum, coda waves show much more fluctuations, confirming the assumptions in section 2.1.

The connection between spectral fluctuations and the emergence of coda waves is well established in radiative transfer theory. The intensity of the wavefield can be expressed as

$$I(\omega, \Omega) \approx \frac{\omega^2 \Delta\omega}{2\pi} \langle u(\omega + \Omega/2) u^*(\omega - \Omega/2) \rangle \qquad (15)$$

where u is the wavefield, ω is the central frequency of the wavefield, $\Delta\omega$ is the bandwidth and Ω is the frequency of the intensity fluctuations (Margerin 2005). $\langle \cdot \rangle$ denotes an ensemble average. Equation 15 states that if the wavefield on the right hand side has a large correlation bandwidth, i.e. its spectrum is correlated over large values of Ω the Intensity on the left hand side has fast fluctuations. A smooth evolution of intensity, i.e. a long lasting coda on the other hand requires the spectral correlation of the wavefield to decay quickly. We can thus conclude that the duration of the coda T is inversely proportional the the correlation bandwidth of the spectrum Ω, i.e.the width of the fluctuations in the spectrum. Based on this relation one can infer from a rough comparison of figures 6c, 11 and 13 that Kilauea likely is the most heterogeneous material since it shows the largest number of fluctuations, i.e. the smallest correlation bandwidth. The strong heterogeneity of volcanic environments is thus the likely reason why the spectral fluctuations have mostly been investigated at volcanoes (Yates et al. 2026) and potentially been misinterpreted as source effects.

Spectral correlation (Eaton et al. 2024) or phase statistics (Anache-Ménier et al. 2009) have been used before to interrogate subsurface heterogeneity based on spectra of coda waves. But the possibility to investigate heterogeneity directly from the spectrum of ambient noise records can complement these approaches with particular benefits in seismically quite regions.

Interestingly Bracale et al. (2025) found that the spectral peaks in their simulations are relatively stable and consistently observed rather independent of the precise source location. Knowing that the Green's functions from different source locations are very different (i.e. uncorrelated, Snieder 2006), why are the fluctuations of the amplitude spectra independent of the source location? Bracale et al. (2025) argue that local resonances for example in fluid-filled cracks generate the consistent spectral lines. And indeed suitably shaped high impedance contrasts certainly generate spectral lines. However, it is not necessary that there are identifiable structures that create resonances. As indicated by Bracale et al. (2025) it suffices that the coda contains *multiply* scattered waves. The travel time τ of waves between any two scatterers is repeatedly sampled by multiply scattered waves which creates fluctuations in the spectrum with a characteristic separation $1/\tau$ irrespective of the source location. Variations of the source location will introduce time shifts of these "echos" and quickly decorrelate the time domain signal. The amplitude spectrum, however, will be unaffected explaining the surprising stability of the fluctuations. Details about the stability of the spectral fluctuations need to be worked out, however, the observations by Bracale et al. (2025) indicate that the monitoring of medium changes from fluctuations of the amplitude spectrum might be less dependent on the source distribution than monitoring with time domain correlation functions.

7 Conclusion

After monitoring subsurface velocity changes for 20 years with ambient noise correlations I show here, that the correlation is in fact not needed and velocity changes can directly be monitored through changes in the amplitude spectrum of the noise. Details about the spatial sensitivity, temporal resolution and dependence of source locations have to be investigated in more detail. But there are obvious technical advantages and the initial thoughts presented here indicate that some methodological advantages might lead to improved temporal resolution and better stability due to a reduced dependence on source signal and location.

Acknowledgements

I thank Luc Illien for providing the measurements of the velocity changes from Nepal. I also thank Alec Yates and Frederik Tilmann for discussion on changes in the noise spectra and comments on the manuscript. This work partially benefited from support by the German Federal Ministry of Research, Technology and Space in the project DEGEREE (03G0925A).

Data availability

Data of the Hawaiian Volcano Observatory station HV.WRM (USGS Hawaiian Volcano Observatory (HVO) 1956) is available at the EarthScope SAGE facility (https://ds.iris.edu/ds/nodes/dmc/). Data from station CX.PATCX (GFZ German Research Centre For Geosciences & Institut Des Sciences De L'Univers-Centre National De La Recherche CNRS-INSU 2006) and the 7F network (Sens-Schönfelder 2023) in Chile as well as data from the XN network (Andermann et al. 2015) in Nepal is available at the GEOFON data center (https://geofon.gfz.de).

References

Anache-Ménier, D., van Tiggelen, B., & Margerin, L., 2009. Phase Statistics of Seismic Coda Waves, *Phys. Rev. Lett.*, **102**(24), 248501, doi: 10.1103/PhysRevLett.102.248501.

Andermann, C., Sens-Schönfelder, C., & Turowski, J., 2015. Landscape response to the mw7.9 gorkha earthquake, doi: 10.14470/KA7560056170.

Ardhuin, F., Stutzmann, E., Schimmel, M., & Mangeney, A., 2011. Ocean wave sources of seismic noise, *J. Geophys. Res. Ocean.*, **116**(9), 1–21, doi: 10.1029/2011JC006952.

Bracale, M., Campillo, M., Shapiro, N. M., Brossier, R., & Melnik, O., 2025. Multiple Scattering of Seismic Waves in a Heterogeneous Magmatic System and Spectral Characteristics of Long Period Volcanic Earthquakes, *J. Geophys. Res. Solid Earth*, **130**(12), 1–18, doi: 10.1029/2025JB031850.

Brenguier, F., Shapiro, N. M., Campillo, M., Ferrazzini, V., Duputel, Z., Coutant, O., & Nercessian, A., 2008. Towards forecasting volcanic eruptions using seismic noise, *Nat. Geosci.*, **1**(2), 126–130, doi: 10.1038/ngeo104.

Brenguier, F., Campillo, M., Takeda, T., Aoki, Y., Shapiro, N. M., Briand, X., Emoto, K., & Miyake, H., 2014. Mapping pressurized volcanic fluids from induced crustal seismic velocity drops, *Science (80-.).*, **345**(6192), 80–82, doi: 10.1126/science.1254073.

Chouet, B. A., 1996. Long-period volcano seismicity: Its source and use in eruption forecasting, *Nature*, **380**(6572), 309–316, doi: 10.1038/380309a0.

Compaire, N., Margerin, L., Monnereau, M., Garcia, R. F., Lange, L., Calvet, M., Dahmen, N. L., Stähler, S. C., Mueller, N., Grott, M., Lognonné, P., Spohn, T., & Banerdt, W. B., 2022. Seasonal variations of subsurface seismic velocities monitored by the SEIS-InSight seismometer on Mars, *Geophys. J. Int.*, **229**(2), 776–799, doi: 10.1093/gji/ggab499.

Curtis, A., Gerstoft, P., Sato, H., Snieder, R., & Wapenaar, K., 2006. Seismic interferometry – turning noise into signal, *Lead. Edge*, **25**(9), 1082, doi: 10.1190/1.2349814.

Dai, S., Wuttke, F., & Santamarina, J. C., 2013. Coda Wave Analysis to Monitor Processes in Soils, *J. Geotech. Geoenvironmental Eng.*, (September), 1504–1511, doi: 10.1061/(ASCE)GT.1943-5606.0000872.

Dinther, C., Margerin, L., & Campillo, M., 2021. Implications of Laterally Varying Scattering Properties for Subsurface Monitoring With Coda Wave Sensitivity Kernels: Application to Volcanic and Fault Zone Setting, *J. Geophys. Res. Solid Earth*, **126**(12), 1–21, doi: 10.1029/2021jb022554.

Eaton, W., Haindl, C., & Nissen-Meyer, T., 2024. Seismic scattering regimes from multiscale entropy and frequency correlations, *Geophys. J. Int.*, **237**(2), 1109–1128, doi: 10.1093/gji/ggae098.

Gassenmeier, M., Sens-Schönfelder, C., Delatre, M., & Korn, M., 2015. Monitoring of environmental influences on seismic velocity at the geological storage site for CO2 in Ketzin (Germany) with ambient seismic noise, *Geophys. J. Int.*, **200**(1), 524–533, doi: 10.1093/gji/ggu413.

Gassenmeier, M., Sens-Schönfelder, C., Eulenfeld, T., Bartsch, M., Victor, P., Tilmann, F., & Korn, M., 2016. Field observations of seismic velocity changes caused by shaking-induced damage and healing due to mesoscopic nonlinearity, *Geophys. J. Int.*, **204**(3), 1490–1502, doi: 10.1093/gji/ggv529.

GFZ German Research Centre For Geosciences & Institut Des Sciences De L'Univers-Centre National De La Recherche CNRS-INSU, 2006. Ipoc seismic network, doi: 10.14470/PK615318.

Hadziioannou, C., Larose, E., Coutant, O., Roux, P., & Campillo, M., 2009. Stability of monitoring weak changes in multiply scattering media with ambient noise correlation: Laboratory experiments, *J. Acoust. Soc. Am.*, **125**, 3688.

Hillers, G. & Ben-Zion, Y., 2011. Seasonal variations of observed noise amplitudes at 2-18 Hz in southern California, *Geophys. J. Int.*, **184**(2), 860–868, doi: 10.1111/j.1365-246X.2010.04886.x.

Illien, L., Andermann, C., Sens-Schönfelder, C., Cook, K. L., Baidya, K. P., Adhikari, L. B., & Hovius, N., 2021. Subsurface Moisture Regulates Himalayan Groundwater Storage and Discharge, *AGU Adv.*, **2**(2), doi: 10.1029/2021av000398.

Illien, L., Sens-Schönfelder, C., Andermann, C., Marc, O., Cook, K. L., Adhikari, L. B., & Hovius, N., 2022. Seismic Velocity Recovery in the Subsurface: Transient Damage and Groundwater Drainage Following the 2015 Gorkha Earthquake, Nepal, *J. Geophys. Res. Solid Earth*, **127**(2), 1–18, doi: 10.1029/2021jb023402.

Illien, L., Sens-Schönfelder, C., & Ke, K. Y., 2023. Resolving minute temporal seismic velocity changes induced by earthquake damage: The more stations, the merrier?, *Geophys. J. Int.*, **234**(1), 124–135, doi: 10.1093/gji/ggad038.

Illien, L., Turowski, J. M., Sens-Schönfelder, C., Berenfeld, C., & Hovius, N., 2025. Predictable recovery rates in near-surface materials after earthquake damage, *Nat. Commun.*, **16**(1), doi: 10.1038/s41467-025-57151-8.

Kanu, C. & Snieder, R., 2015. Time-lapse imaging of a localized weak change with multiply scattered waves using numerical-based sensitivity kernel, *J. Geophys. Res. Solid Earth*, **120**(8), 5595–5605, doi: 10.1002/2015JB011871.

Larose, E., Planes, T., Rossetto, V., & Margerin, L., 2010. Locating a small change in a multiple scattering environment, *Appl. Phys. Lett.*, **96**(20), 204101, doi: 10.1063/1.3431269.

Lindner, F., Wassermann, J., & Igel, H., 2021. Seasonal Freeze-Thaw Cycles and Permafrost Degradation on Mt. Zugspitze (German/Austrian Alps) Revealed by Single-Station Seismic Monitoring, *Geophys. Res. Lett.*, **48**(18), 1–11, doi: 10.1029/2021GL094659.

Lobkis, O. I. & Weaver, R. L., 2003. Coda-Wave Interferometry in Finite Solids: Recovery of [Formula presented]-to-[Formula presented] Conversion Rates in an Elastodynamic Billiard, *Phys. Rev. Lett.*, **90**(25), 4, doi: 10.1103/PhysRevLett.90.254302.

Makus, P. & Sens-Schönfelder, C., 2024. SeisMIC - an Open Source Python Toolset to Compute Velocity Changes from Ambient Seismic Noise, *Seismica*, **3**, doi: 10.26443/seismica.v3i1.1099.

Makus, P., Denolle, M. A., Sens-Schönfelder, C., Köpfli, M., & Tilmann, F., 2024. Analyzing Volcanic, Tectonic, and Environmental Influences on the Seismic Velocity from 25 Years of Data at Mount St. Helens, *Seismol. Res. Lett.*, **95**(5), 2674–2688, doi: 10.1785/0220240088.

Mao, S., Lecointre, A., Hilst, R. D. V. D., & Campillo, M., 2022. Space-time monitoring of groundwater fluctuations with passive seismic interferometry, *Nat. Commun.*, pp. 1–9, doi: 10.1038/s41467-022-32194-3.

Margerin, L., 2005. Introduction to radiative transfer of seismic waves, in *Seism. data Anal. with Glob. local arrays*, vol. 157, pp. 229–252, eds Levander, A. & Nolet, G., AGU AMERICAN GEOPHYSICAL UNION.

Nakata, N. & Snieder, R., 2012. Estimating near-surface shear wave velocities in Japan by applying seismic interferometry to KiK-net data, *J. Geophys. Res.*, **117**(B1), B01308, doi: 10.1029/2011JB008595.

Obermann, A., Planes, T., Larose, E., Sens-Schönfelder, C., & Campillo, M., 2013. Depth sensitivity of seismic coda waves to velocity perturbations in an elastic heterogeneous medium, *Geophys. J. Int.*, doi: 10.1093/gji/ggt043.

Pacheco, C. & Snieder, R., 2005. Time-lapse travel time change of multiply scattered acoustic waves, *J. Acoust. Soc. Am.*, **118**(3), 1300, doi: 10.1121/1.2000827.

Pacheco, C. & Snieder, R., 2006. Time-lapse traveltime change of singly scattered acoustic waves, *Geophys. J. Int.*, **165**(2), 485–500, doi: 10.1111/j.1365-246X.2006.02856.x.

Poupinet, G., Ellsworth, W., & Frechet, J., 1984. Monitoring Velocity Variations in the Crust Using Earthquake Doublets: An Application to the Calaveras Fault, California, *J. Geophys. Res.*, **89**(4), 5719–5731.

Ratdomopurbo, A. & Poupinet, G., 1995. Monitoring a temporal change of seismic velocity in a volcano: Application to the 1992 eruption of Mt. Merapi (Indonesia), *Geophys. Res. Lett.*, **22**(7), 775–778, doi: 10.1029/95GL00302.

Richter, T., Sens-Schönfelder, C., Kind, R., & Asch, G., 2014. Comprehensive observation and modeling of earthquake and temperature-related seismic velocity changes in northern Chile with passive image interferometry, *J. Geophys. Res.*, **119**, 4747–4765, doi: 10.1002/2013JB010695.

Sato, H., Fehler, M., & Maeda, T., 2012. *Seismic Wave Propagation and Scattering in the Heterogeneous Earth*, Springer, Heidelberg, 2nd edition.

Sens-Schönfelder, C. & Brenguier, F., 2019. Noise-based Monitoring, in *Seism. Ambient Noise*, chap. 9, pp. 267–301, eds Nakata, N., Gualtieri, L., & Fichtner, A., Cambridge University Press.

Sens-Schönfelder, C. & Eulenfeld, T., 2019. Probing the in

situ elastic nonlinearity of rocks with earth tides and seismic noise, *Phys. Rev. Lett.*, **122**(13), 138501, doi: 10.1103/PhysRevLett.122.138501.
Sens-Schönfelder, C. & Larose, E., 2010. Lunar noise correlation, imaging and monitoring, *Earthq. Sci.*, **23**(5), 519–530, doi: 10.1007/s11589-010-0750-6.
Sens-Schönfelder, C. & Wegler, U., 2006. Passive image interferometry and seasonal variations of seismic velocities at Merapi Volcano, Indonesia, *Geophys. Res. Lett.*, **33**(21), L21302, doi: 10.1029/2006GL027797.
Sens-Schönfelder, C., Pomponi, E., & Peltier, A., 2014. Dynamics of Piton de la Fournaise Volcano Observed by Passive Image Interferometry with Multiple References, *J. Volcanol. Geotherm. Res.*, **276**, 32–45, doi: 10.1016/j.jvolgeores.2014.02.012.
Sens-Schönfelder, C., Snieder, R., & Stähler, S. C., 2015. The lack of equipartitioning in global body wave coda, *Geophys. Res. Lett.*, **42**, 7483–7489, doi: 10.1002/2015GL065108.
Sens-Schönfelder, C., 2023. Patache stress observation (peso), doi: 10.14470/2S162326.
Snieder, R., 2006. The Theory of Coda Wave Interferometry, *Pure Appl. Geophys.*, **163**(2-3), 455–473, doi: 10.1007/s00024-005-0026-6.
Snieder, R. & Larose, E., 2013. Extracting Earth's Elastic Wave Response from Noise Measurements, *Annu. Rev. Earth Planet. Sci.*, **41**(1), 183–206, doi: 10.1146/annurev-earth-050212-123936.
Snieder, R., Grêt, A., Douma, H., & Scales, J., 2002. Coda wave interferometry for estimating nonlinear behavior in seismic velocity., *Science*, **295**(5563), 2253–5, doi: 10.1126/science.1070015.
Snieder, R., Wapenaar, K., & Wegler, U., 2007. Unified Green's function retrieval by cross-correlation; Connection with energy principles, *Phys. Rev. E - Stat. Nonlinear, Soft Matter Phys.*, **75**(3), doi: 10.1103/PhysRevE.75.036103.
Takano, T., Nishimura, T., Nakahara, H., Ohta, Y., & Tanaka, S., 2014. Seismic velocity changes caused by the earth tide: ambient noise correlation analyses of a small array data, *Geophys. Res. Lett.*, pp. 6131–6136, doi: 10.1002/2014GL060690.
USGS Hawaiian Volcano Observatory (HVO), 1956. Hawaiian volcano observatory network, doi: 10.7914/SN/HV.
Wang, Q. Y., Brenguier, F., Campillo, M., Lecointre, A., Takeda, T., & Aoki, Y., 2017. Seasonal Crustal Seismic Velocity Changes Throughout Japan, *J. Geophys. Res. Solid Earth*, **122**(10), 7987–8002, doi: 10.1002/2017JB014307.
Wegler, U. & Sens-Schönfelder, C., 2007. Fault zone monitoring with passive image interferometry, *Geophys. J. Int.*, **168**(3), 1029–1033, doi: 10.1111/j.1365-246X.2006.03284.x.
Wegler, U., Lühr, B.-G., Snieder, R., & Ratdomopurbo, A., 2006. Increase of shear wave velocity before the 1998 eruption of Merapi volcano (Indonesia), *Geophys. Res. Lett.*, **33**, 9303, doi: 10.1029/2006GL025928.
Yamamura, K., Sano, O., Utada, H., Takei, Y., Nakao, S., & Fukao, Y., 2003. Long-term observation of in situ seismic velocity and attenuation, *J. Geophys. Res. Solid Earth*, **108**(B6), 1–15, doi: 10.1029/2002JB002005.
Yamaoka, K., Kunitomo, T., Miyakawa, K., Kobayashi, K., & Kumazawa, M., 2001. A trial for monitoring temporal variation of seismic velocity using an ACROSS system, *Isl. Arc*, **10**(3-4), 336–347, doi: 10.1111/j.1440-1738.2001.00332.x.
Yates, A. S., Heuninck, S., Barajas, A., Bektas, H., Caudron, C., De Angelis, S., & Zuccarello, L., 2026. Tracking Subsurface Changes via Frequency Shifts in Volcanic Tremor Spectral Lines: Observations From Mt Etna, *Geophys. Res. Lett.*, **53**(2), 1–12, doi: 10.1029/2025GL117819.
Zhan, Z., Tsai, V. C., & Clayton, R. W., 2013. Spurious velocity changes caused by temporal variations in ambient noise frequency content, *Geophys. J. Int.*, **194**(3), 1574–1581, doi: 10.1093/gji/ggt170.
Zhang, T. & Sens-Schönfelder, C., 2022. Adjoint envelope tomography for scattering and absorption using radiative transfer theory, *Geophys. J. Int.*, **229**(1), 566–588, doi: 10.1093/gji/ggab457.
Zhang, T., Sens-Schönfelder, C., & Margerin, L., 2021. Sensitivity kernels for static and dynamic tomography of scattering and absorbing media with elastic waves: a probabilistic approach, *Geophys. J. Int.*, pp. 1824–1853, doi: 10.1093/gji/ggab048.